ARMA 22–2261

The EGS Collab Project – Stimulations at Two Depths

Kneafsey, T.J., Dobson, P.F., Ulrich, C., Hopp, C., Rodríguez-Tribaldos, V., and Guglielmi, Y.
Lawrence Berkeley National Laboratory, Berkeley, California, USA
Blankenship, D., Schwering, P.C., and Ingraham M.
Sandia National Laboratories, Albuquerque, New Mexico, USA
Burghardt, J.A., White, M.D., Johnson, T.C., Strickland, C., Vermuel, V., and Knox, H.A.
Pacific Northwest National Laboratory, Richland, Washington, USA
Morris, J.P., Fu, P., Smith, M., and Wu, H.
Lawrence Livermore National Laboratory, Livermore, California, USA
Ajo-Franklin, J.B.
Rice University, Houston, Texas, USA
Huang, L.
Los Alamos National Laboratory, Los Alamos, New Mexico, USA
Neupane, G.
Idaho National Laboratory, Idaho Falls, Idaho, USA
Horne, R.
Stanford University, Stanford, California, USA
Roggenthen, W.
South Dakota School of Mines and Technology, Rapid City, South Dakota, USA
Weers, J.
National Renewable Energy Laboratory, Golden Colorado, USA
Doe, T.W.
TDoeGeo, Bellvue, Washington, USA
Pyatina, T.
Brookhaven National Laboratory, Upton, NY, USA
The EGS Collab Team*

This paper was prepared for presentation at the 56th US Rock Mechanics/Geomechanics Symposium held in Santa Fe, New Mexico, USA, 26-29 June 2022. This paper was selected for presentation at the symposium by an ARMA Technical Program Committee based on a technical and critical review of the paper by a minimum of two technical reviewers. The material, as presented, does not necessarily reflect any position of ARMA, its officers, or members. Electronic reproduction, distribution, or storage of any part of this paper for commercial purposes without the written consent of ARMA is prohibited. Permission to

ABSTRACT: The EGS Collab project, supported by the US Department of Energy, is performing intensively monitored rock stimulation and flow tests at the 10-m scale in an underground research laboratory to address challenges in implementing enhanced geothermal systems (EGS). Data and observations from the field tests are compared to simulations to understand processes and build confidence in numerical modeling of the processes. We have completed Experiment 1 (of 3), which examined hydraulic fracturing in a well-characterized underground fractured phyllite test bed at a depth of approximately 1.5 km at the Sanford Underground Research Facility (SURF) in Lead, South Dakota. Testbed characterization included fracture mapping, borehole acoustic and optical televiewers, full waveform sonic, conductivity, resistivity, temperature, campaign p- and s-wave investigations and

electrical resistance tomography. Borehole geophysical techniques including passive seismic, continuous active source seismic monitoring, electrical resistance tomography, fiber-based distributed strain, distributed temperature, and distributed acoustic monitoring, were used to carefully monitor stimulation events and flow tests. More than a dozen stimulations and nearly one year of flow tests were performed. Quality data and detailed observations were collected and analyzed during stimulation and water flow tests using ambient temperature and chilled water. We achieved adaptive control of the tests using real-time monitoring and rapid dissemination of data and near-real-time simulation. More detailed numerical simulation was performed to answer key experimental design questions, forecast fracture propagation trajectories and extents, and analyze and evaluate results. Data are freely available from the Geothermal Data Repository.

Experiment 2 examines the potential for hydraulic shearing in amphibolite at a depth of about 1.25 km at SURF. This site has a different set of stress and fracture conditions than Experiment 1. The Experiment 2 testbed consists of nine subhorizontal boreholes configured in two fans of two boreholes which surround the testbed and contain grouted-in electrical resistance tomography, seismic sensors, active seismic sources and distributed fiber sensors. A "five-spot" set of test wells that extends from a custom mined alcove includes an injection well and four production/ monitoring wells. The testbed was characterized geophysically and hydrologically, and three stimulations have been performed using the Step-Rate Injection Method for Fracture In-Situ Properties (SIMFIP) tool to measure strains, and a new strain quantifying tool (downhole robotic strain analysis tool -DORSA) was deployed in a monitoring hole during stimulation. Real-time data were broadcast during stimulations to allow real-time response to arising issues.

1. INTRODUCTION

Enhanced or engineered geothermal systems (EGS) offer tremendous potential as a clean, renewable energy resource. Estimates exceed 500 GWe for the western US, surpassing the resource base hosted by conventional hydrothermal systems (Williams et al., 2008). For the entire United States EGS resource estimates range up to an order of magnitude larger (Augustine, 2016). Implementing EGS will be expedited by (1) improving the understanding and efficacy of stimulation techniques under appropriate in-situ conditions allowing communication among multiple wells, (2) improving imaging and monitoring techniques for permeability enhancement and evolution, as well as associated microseismicity, (3) improving technologies for zonal isolation for multistage stimulations under elevated temperatures, (4) developing technologies to isolate zones for controlling fast flow paths and control early thermal breakthrough, and (5) developing scientifically-based long-term EGS reservoir sustainability and management techniques.

The EGS Collab project aims to advance our understanding of rock mass response to stimulation using accessible deep rock under stress relevant to EGS. Our 10-m spatial scale tests and analyses support validation of thermal-hydrological-mechanical-chemical (THMC) modeling. We are also testing and improving conventional and novel field monitoring tools. We focus on understanding and predicting permeability enhancement and evolution in crystalline rock, including how to create sustained and distributed permeability for heat extraction from a reservoir by generating new fractures that complement existing fractures. The project has planned three multi-test experiments to increase understanding of 1) hydraulic fracturing (Experiment 1- complete), 2) shear stimulation (Experiment 2 –underway), and 3) other stimulation methods in Experiment 3. The testbeds where the experiments are conducted are first characterized to provide detailed information on their geology, fracture distribution and orientation, stress regime, and basic rock properties. Each series of tests within an experiment begins with modeling to support experiment design, and post-test modeling and analysis are performed to examine the effectiveness of our modeling and monitoring tools and approaches. By doing this, we can gain confidence in EGS prediction and improve the array of modeling and monitoring tools in use.

Experiment 1 was performed on the 4850 (foot depth, ~1.5 km) level at the Sanford Underground Research Facility (SURF, Figure 1) in Lead, South Dakota (Heise, 2015). This experiment established a fracture network connecting an injection well and a production well using hydraulic fracturing (Morris et al., 2018). The test bed consisted of eight ~60 m long continuously-cored subhorizontal boreholes. The boreholes were characterized using optical and acoustic televiewers, full waveform sonic, electrical resistivity, natural gamma, and temperature/conductivity logs (Ulrich et al., 2018). Six boreholes surrounding the experimental volume of rock contained grouted-in sensors (Kneafsey et al., 2020). Monitoring systems included electrical resistivity tomography (Johnson et al., 2019; Johnson et al., 2021), continuous active source seismic monitoring and passive seismic monitoring (CASSM) (Ajo-Franklin et al., 2018; Chai et al., 2020; Chi et al., 2020; Fu et al., 2019; Fu et al., 2021; Pan et al., 2019; Schoenball et al., 2019; Schoenball et al., 2020a; Schoenball et al., 2020b; Schoenball et al., 2021; Templeton et al., 2019), distributed temperature, strain, and acoustic monitoring (Fu et al., 2021). Our understanding of the local stress regime was based on kISMET Project field characterizations (Oldenburg et al., 2017; Wang et al., 2017). The injection and production boreholes are oriented approximately parallel to the minimum principal stress direction. This was done so that hydraulic fractures would tend to propagate orthogonally to the injection well. More than a dozen stimulations were performed and the injection and production boreholes were connected in multiple locations (White et al., 2019). Flow tests were conducted using ambient temperature water initially, and then chilled water (to model EGS) over the course of a year (Kneafsey et al., 2021). Numerous tracer tests were performed to understand flow conditions (Mattson et al., 2019a; Mattson et al., 2019b; Neupane et al., 2020; Wu et al., 2019).

All tests were analyzed before and after using a range of models (Fu et al., 2021; Jafarov et al., 2020; Makedonska et al., 2020; White et al., 2019; White et al., 2021; White et al., 2020; White et al., 2018) to better understand how to model the processes observed. Additional details on Experiment 1 are also available (e.g., Dobson et al. (2021); Kneafsey et al. (2021); White et al. (2019), Google Scholar, author “EGS Collab”) and data sets are available (https://gdr.openei.org/egs_collab).

Experiment 2 investigates shear stimulation. The testbed for this experiment is on the 4100 (foot depth, ~1.25 km) level at SURF in the Yates amphibolite and the subsurface stress conditions are different from those of Experiment 1 on the 4850 level (Ingraham et al., 2020). Analyses have been performed to understand shearing in this testbed (Dobson et al., 2018; Ingraham et al., 2020; Meng et al., 2021a; Meng et al., 2021b; Singh et al., 2019). Pre-test investigation of the 4100 level included mapping fractures and features that can be observed on the drift walls, and the drilling and logging of a 10 m horizontal borehole and a 50 m vertical borehole. The vertical borehole identified and penetrated an 11 m thick rhyolite layer. Eighteen stress tests were performed in the vertical borehole (eight of these have used the Step-Rate Injection Method for Fracture In-Situ Properties (SIMFIP) tool (Guglielmi et al., 2015; Guglielmi et al., 2021a; Guglielmi et al., 2021b; Guglielmi et al., 2022; Guglielmi et al., 2014)) to quantify displacement during testing. These tests showed significant stress heterogeneity, with instantaneous shut-in pressures (ISIP - indicating minimum principal stress information) in the amphibolite below the rhyolite around 27.6 MPa (4000 psi), wihtin the rhyolite around 18.6 MPa (2700 psi), and in the upper amphibolite around 21.4 MPa (3100 psi). Because of this stress heterogeneity, the Experiment 2 test bed is designed to be entirely above this rhyolite layer.

In addition to the geologic and characterization information from the two characterization boreholes, the site geology was further investigated including mapping observed fractures and features on the drift walls and boreholes (Section 2). This information informed preliminary testbed design. The testbed was configured based on geologic and stress knowledge, shear probabilities, and budget

(Section 3). Boreholes were cored and characterized geologically (including core examination), geophysically, and hydrologically to refine test design and monitoring system design (Sections 2 and 4). Monitoring system design was informed by Experiment 1 performance and numerical simulation to optimize data quality (Section 5). All the previous steps informed the stimulation plan, and the stimulation and flow system design (Section 6). The result is a well-characterized testbed optimized to encourage shear stimulation and quantify the effectiveness of the stimulation and the resulting ability to effectively perform EGS-related flow tests providing high-quality data for model and code validation.

2. GEOLOGY

Our understanding of the Experiment 2 testbed geology initiated with published and unpublished reports and information from data archives. Viewing our site from the perspective of EGS, we enhanced our understanding by detailed mapping of fractures in the drift, and examination of core and borehole logs from our characterization boreholes TV4100 and TH4100. Upon coring our nine test boreholes, we gathered significant new data to understand our site, fracture sets, fracture fills, and orientations.

The general geology in the vicinity of Experiments 1 and 2 is dominated by an anticline that plunges to the southeast (Lisenbee & Terry, 2009). The Testbed 1 (on the 4850 level) host rock on the west flank of the anticline was entirely within a carbonate-mica phyllite metasedimentary rock of the upper Poorman Formation, described more fully in Caddey et al. (1991). Stratigraphically, this metasedimentary rock overlies an older amphibolite sequence called the Yates member of the Poorman Formation, which is the host rock for the testbed on the 4100 level. Experiment 2 is located on the same anticline as Testbed 1 but it is nearer to the crest of the anticline (Figure 1). The Yates member consists of metamorphosed basalts and volcaniclastic sediments, forming a massive hornblende-plagioclase amphibolite schist, with lesser amounts of chlorite, quartz, and calcite (Caddey et al., 1991; Lisenbee & Terry, 2009). Several thin, sulfur-rich layers are exposed in the access drift near Testbed 2. These features are oxidized where visible but presumably contain unoxidized sulfides within the rock. These features represent geomechanically weak intervals and may reflect original bedding.

The host rock for both experiments is of Precambrian age, yet a Paleogene (Tertiary) rhyolite occurs near and beneath the Testbed 2 volume. This rhyolite body is exposed in both the drift and in a vertical reconnaissance borehole, TV4100 (drilled in 2019), which intersected this shallow-dipping rhyolite dike in a similar orientation to the exposures of rhyolite on the 4100 Level near the Yates shaft (Figure 1).

Detailed mapping of fractures in the drift and the nearby Battery Alcove was performed to determine the nature and orientation of visible fractures. Three main classes of fractures were identified: foliation-parallel features, conjugate shear sets, and larger fractures interpreted to be Tertiary features associated with rhyolite dike emplacement. Figure 2 shows the relation between the thin healed fractures of probable Precambrian age and a much larger Tertiary-age fracture. The higher angle fractures in Figure 2 possess infrequent small pore spaces of unknown connectivity, whereas the thin healed fractures do not provide such evidence.

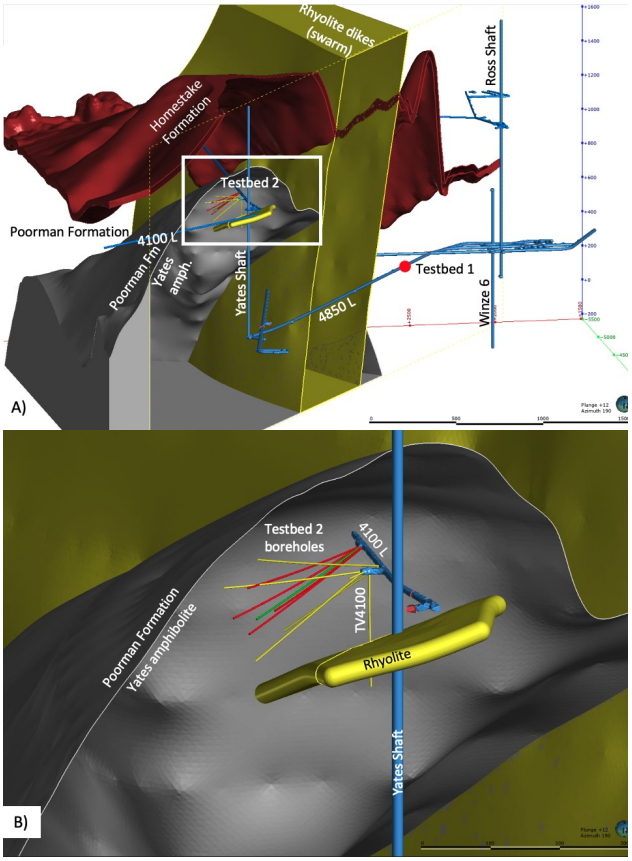

Figure 1. A. Representation of the geology of the rock hosting Testbeds 1 and 2. B. Enlarged region showing Testbed 2, the host rock, and location of the rhyolite. Experiment 2 testbed monitoring wells are yellow, and test wells are red and green. The proposed injection well is green.

Core examination

Continuous core samples were collected from each of nine testbed boreholes. The cores were logged and described during drilling operations, with selected intervals re-examined at the surface. Significant differences in the rock fabric from Testbed 1 and Testbed 2 were observed (Figure 3) due to the different modes of formation, i.e., layered sedimentary deposits as opposed to an igneous origin for the amphibolite.

Experiment 2 core examination results were consistent with the observations made in the drifts (Figure 2). Most fractures observed in the core were healed and filled with quartz, calcite, and minor sulfides. Small vugs (<0.5 mm) were observed infrequently, and testing using a hand-held permeameter yielded only limited connectivity. However, in several intervals the amphibolite was heavily altered, presumably related to the intrusion of nearby rhyolite. The altered amphibolite is a greenish-gray color with numerous small healed fractures. In two notable instances, however, large open fractures have been preserved (Figure 4). The degree of shearing associated with the alteration varies from none to at least one instance where the central portion of this zone exhibits a plastic clay-like behavior.

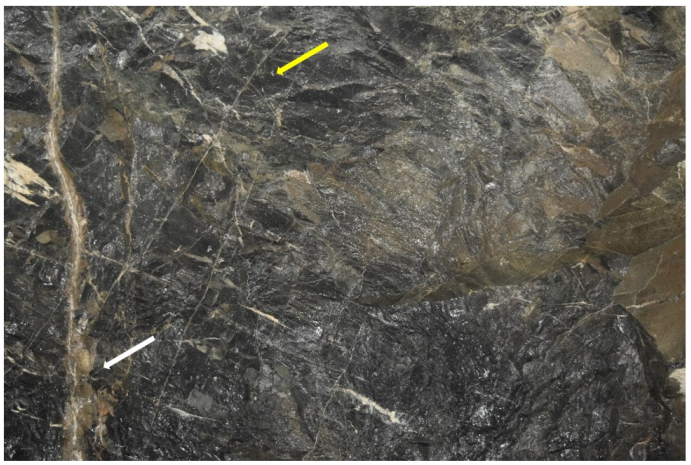

Figure 2. Fractures observed in the Battery Alcove on the 4100 level. White arrow points to large Tertiary fracture that can be traced over 5 m within the alcove and drift; yellow arrow indicates an example of a conjugate shear set.

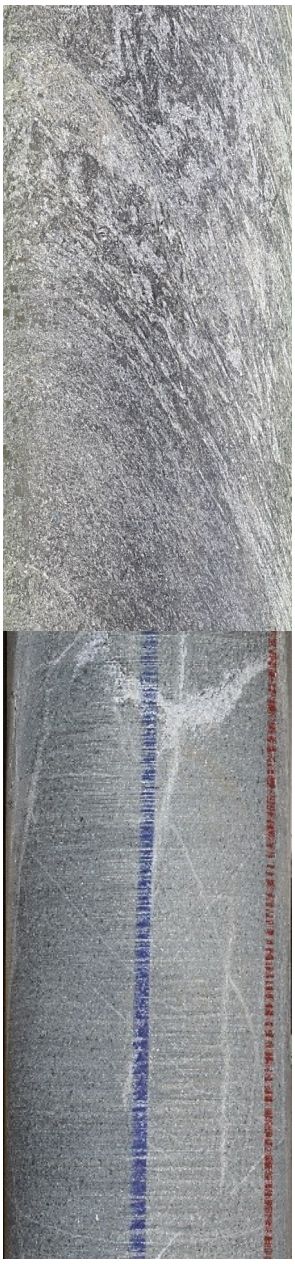

Figure 3. Example of core from Experiment 1 testbed (left) and Experiment 2 testbed (right). The carbonate mica phyllite in Experiment 1 shows prominent layering whereas the amphibolite from Experiment 2 is massive with many healed fractures.

More detailed fracture analysis has been conducted on optical and acoustic televiewer logs collected from all new testbed boreholes described below. These data are used to identify appropriate intervals within the main injection borehole (E2-TC) to attempt hydraulic shear stimulation.

3. EXPERIMENT 2 DESIGN

Our goal in constructing the Experiment 2 testbed was to hydraulically shear fractures to create appropriate EGS-useful permeability. To do so, we needed to identify appropriate fracture sets that may shear under designed stimulation conditions, drill boreholes that intersect those fracture sets optimally, and place boreholes to enable monitoring using conventional and new and unique equipment.

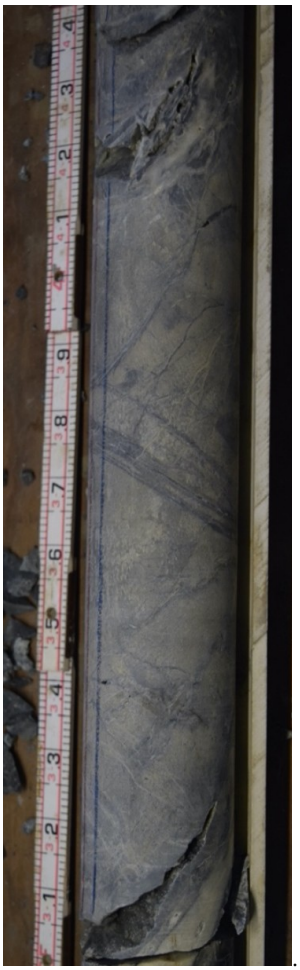

Figure. 4. Core photo of E2-AML at ~187 feet deep, showing some open portions of a highly fractured interval.

One of the first design considerations for Experiment 2 was the reduced space available on the 4100 level drifts. For Experiment 1, we were able to utilize a wide, double-track portion of a drift on the 4850 level for the entire length of the testbed. This allowed us to avoid any additional excavation to accommodate drilling, stimulation, flow, and monitoring equipment. Figure 5 shows schematically two of the options that were considered for utilizing space on the 4100 level. Note that in the sections that are not double track, the nominal drift width and height is about 2.1 m (7 ft). To avoid costly mining, a concept was developed that would utilize a limited stretch of double track in combination with a preexisting battery alcove (Figure 5, left). While reducing the cost, this approach would have multiple

disadvantages, including limited space margins in the battery alcove and the necessity that significant tubing and cabling be run down the drift between the double-track and the battery alcove. Other options included several excavations to extend the battery alcove and construct two additional alcove areas to accommodate stimulation and monitoring equipment (Figure 5, right). The final design was similar to that shown in Figure 5 (right) without extending the Battery Alcove.

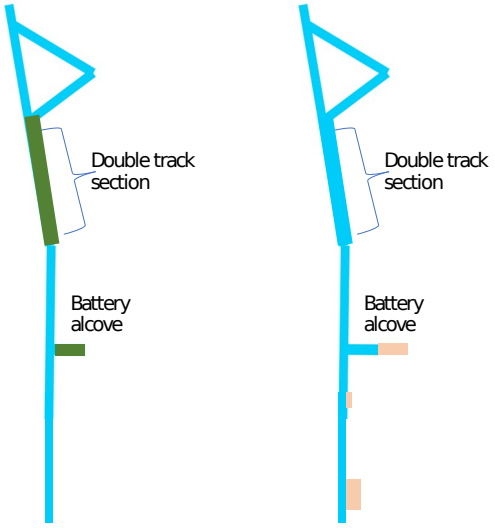

Figure 5: Plan view of options for experimental design on the 4100 level. No additional excavation (left) and significant excavation (right). Ultimately, the project was able to support a design similar to that on the right. Green areas correspond to preexisting portions of the drift complex. The peach areas indicate potential excavations.

The orientations of the injection and production wells were selected to increase the likelihood of intersecting natural fractures that are favorably oriented for shear reactivation. The analysis considered five fracture set orientations () identified from the drift wall and borehole observations. We developed a model of the stress field based upon observations from the characterization wells and estimated a minimum horizontal stress of 18.3 MPa with an azimuth of 24 degrees, dipping 28 degrees from the horizontal. The maximum horizontal stress, vertical stress and pore pressure were estimated to be 37.3 MPa, 36 MPa, and 4.23 MPa, respectively. Figure 6 shows the estimated slip tendency for the five joint sets under this assumed stress state. We observe that sets 1, 4, and 5 are oriented most favorably for shear activation. During the design phase, the specific locations of fractures were not known as drilling had not been completed. Because of that, it was decided to have multiple production wells (E2-TL, E2-TU, E2-TN, E2-TS, where “T” stands for “test”. “L” for lower, “U” for upper, “N” for north, and “S” for south) surrounding the injection well (E2-TC, “C” for center), (Figure 7). In this manner, it can be expected that stimulated fractures will intersect at least one production well.

For design purposes, equal numbers of fractures from each joint set were randomly placed within the stimulated volume. In Figure 7 we only show fractures (disks) that intersect the injection and production wells, and hotter colors indicate greater slip tendency. Figure 7 indicates that this design is expected to intersect mostly fractures within JS1, which we have estimated to have high slip tendency (Figure 6). Analyses were performed using the Fat Crayon Toolkit (Morris, 2021).

Schematics of the Experiment 2 well layout are shown in Figures 1, 7, and 12. In this testbed, the production borehole(s) (red) fan out surrounding the injection well to provide different distances between the wells depending on the depth from the collar. Production wells not intersected by stimulated fractures will also be used as an ungrouted monitoring wells. Monitoring wells (E2-DMU, E2-DML, E2-AMU, E2-AML, where “D” stands for drift, “A” for alcove, and “M” for monitoring) are oriented to encompass the volume of interest on as many sides as possible at a larger distance than was used in Experiment 1. In this configuration we have two pairs of monitoring wells oriented approximately orthogonal to the injection well above and below the stimulation zone. The variety of sensors deployed in Experiment 2 will be similar to those in Experiment 1, but their layout and robustness (e.g., tubing encapsulated cable) have been improved based on learnings from Experiment 1. (See Monitoring System Design below).

Table 1: Five fracture set orientations were identified and were considered during design of Experiment 2.

Name	Strike	Dip
JS1	155.0	55.0
JS2	20.0	27.0
JS3	280.0	50.0
JS4	265.0	70.0
Sulfide layer (JS5)	50.0	40.0

Extensive simulations of hydraulic stimulations were performed during the Experiment 2 design phase. In addition to shear stimulation, we also considered hydraulic fracturing. This is because the outcome of hydraulic shearing depends highly on in situ characteristics of natural fractures known to be highly variable and difficult to measure. Because the uncertainties in the simulation parameters are greater than the value of hydraulic shearing simulations in the design phase, we focused on two simulation tasks that can directly impact testbed design decisions:

1. Predict the propagation trajectory of a potential opening-mode hydraulic fracture.

2. Predict the breakdown pressure in the near-wellbore region for identified natural fractures.

Detailed results on the first simulation task were reported in (Fu et al., 2021). Results on the second task are presented in Burghardt et al. (2022)

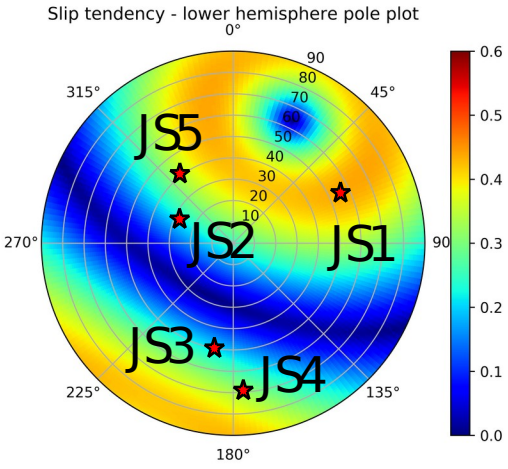

Figure 6: Slip tendency plot for the five identified joint sets. The slip tendency is the coefficient of friction required to avoid slip under the assumed stress conditions. Consequently, higher slip tendency (warmer colors) indicates an orientation closer to slip. For the assumed stress state, sets 1, 4, and 5 are oriented most favorably for slip.

4. TESTBED CHARACTERIZATION

Our characterization is key in gaining further insights into our testbed. To better understand the rock and environment, we used conventional wireline tools such as optical and acoustic televiewers, full waveform sonic, conductivity and temperature, and resistivity. Hydrological characterization was performed by pressurizing intervals using straddle packers to ascertain local and fracture permeability, and connectivity between wells.

Wireline Characterization

A suite of geophysical wireline tools was used to characterize the rock and fractures within the Experiment 2 testbed. Understanding the thermal gradient away from the drift is important, as are the changes in rock types within the testbed, fracture types (including healed, open, flowing), rock foliation, formation fluid conductivity, rock resistivity and acoustic velocities, and the final borehole orientations. To collect this information, we used a Mt. Sopris logging system that coupled a Matrix data logging unit to a series of downhole geophysical probes: Fluid Temperature and Conductivity, Optical and Acoustic Borehole Imaging, Electrical Resistivity, Full Waveform Sonic, and a North-seeking gyro by Axis Mining Technology. Logs from these tools were run in all 9 boreholes, as well as the TV4100 characterization borehole, resulting in 56 high resolution log data sets. Temperatures near the drift in well TC (likely stimulation well) started around 25°C and increased to around 30°C at the end of the borehole, 80 m from the drift. This gradient is not as steep as the gradient observed in the Experiment 1 testbed, consistent with lower background rock temperatures expected at the shallower drift depth and higher wall temperature from less extensive ventilation. Rock resistivities ranged from 100 – 100k Ohm-m. Natural gamma spikes at changes in rock types and/or at fractures with fine fault-gouge sediments were observed along with associated resistivity decreases (Figure

8). Gamma spikes are generally associated with increases in clay content and/or potassium-bearing rocks or fractures. Near-wellbore acoustic velocities were estimated with a three-receiver unit. P-wave velocities range from 5,000 – 8,000 m/s and shear wave velocities range from approximately 2,500 – 4,000 m/s. The optical and acoustic borehole imagers captured numerous fractures throughout the length of each borehole, resulting in approximately 1300 fractures (healed and open fractures, filled veins, etc.) that were picked to identify fracture sets with specific orientations which would be used in a slip tendency analysis to select favorable fractures for later stimulations. These fractures can also be used to develop a discrete fracture network model. An example of some picked fractures is shown in Figure 9.

Hydraulic Characterization

The testbed is located 4100 ft (1250 m) below ground surface (bgs) with the nominal water table located at 80.7 m below the ground surface, yielding a potential hydrostatic pore pressure of 11.47 MPa. Earlier mining operations, prior to closure of the Homestake Mine in 2002, included active water pumping to 8,000 ft (2,438 m) bgs (the current water level at SURF is ~5700 ft bgs). The testbed is located laterally near the vertical Yates shaft (Figure1), which was started in 1938 and extends to about 5000 ft, thus the testbed is probably within the drained region. This level (unlike the 4850) did not experience reflooding during the time between when commercial mining operation ceased and the facility was converted to an underground research laboratory (Zhan & Duex, 2010). The current pore pressure in the region of the test bed is heterogenous. The hydrostatic head to the shallow water table provides an upper limit to the pore pressure at the 4100 level of about 12 MPa; however, pore pressure measurements in boreholes drilled for the DUSEL experiment at the 4850 level (Stetler, 2015) showed that most were non-flowing and the three that did flow yielded pore pressures that were between 15% and 60% of hydrostatic.

In the Experiment 2 test bed area there are weeping fractures along the drift in rhyolite about100 m from the testbed near the Poorman-Yates formation contact. A vertical exploration hole for our Experiment 2 produced less than 0.1 liter/min water from a fracture in a rhyolite dike at a pressure measured as high as 200 psi (1.4 MPa or ~11% of hydrostatic. Note that the well was vented at 200 psi, that is not the well pressure.). Of the Experiment 2 boreholes only one produced water with a rate of ~ 0.2 l/min, however no shut-in pressure was recorded.

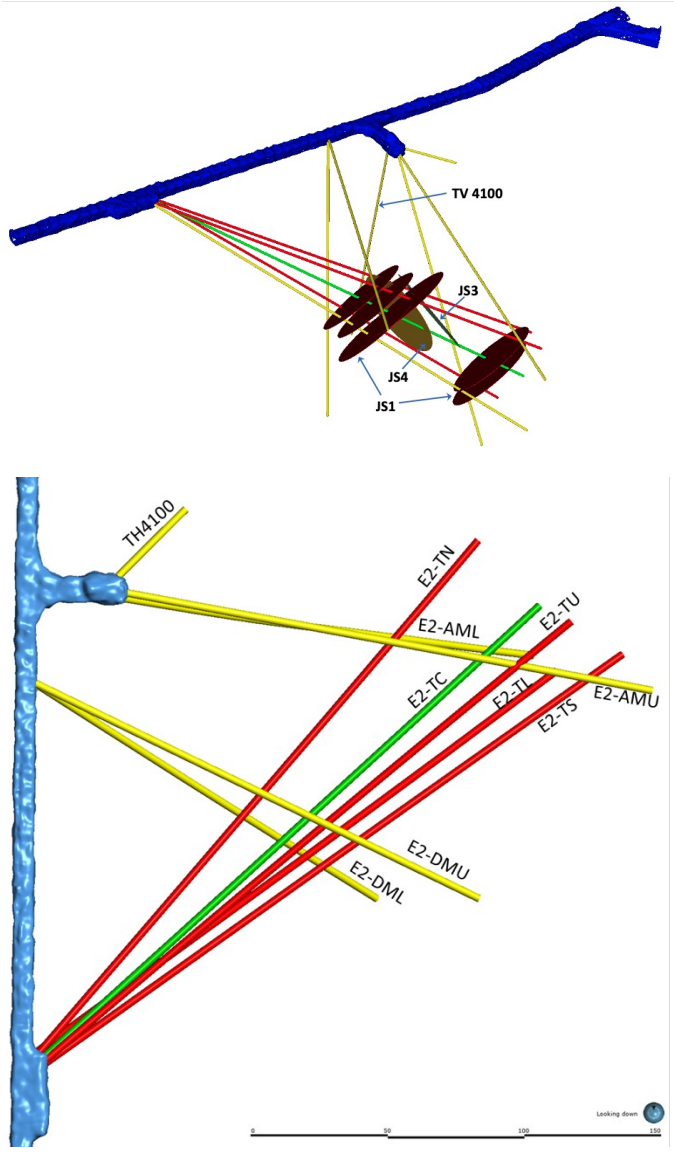

Figure 7. Well orientations for Experiment 2. The thick blue object represents the drift, the green line represents the injection well, red lines represent production wells, and yellow lines represent monitoring wells. Other than the vertical well TV4100,

all wells are subhorizontal. Disks in the top figure indicate potential natural fractures sets that connect the injection and projection wells and hotter colors indicate greater slip tendency.

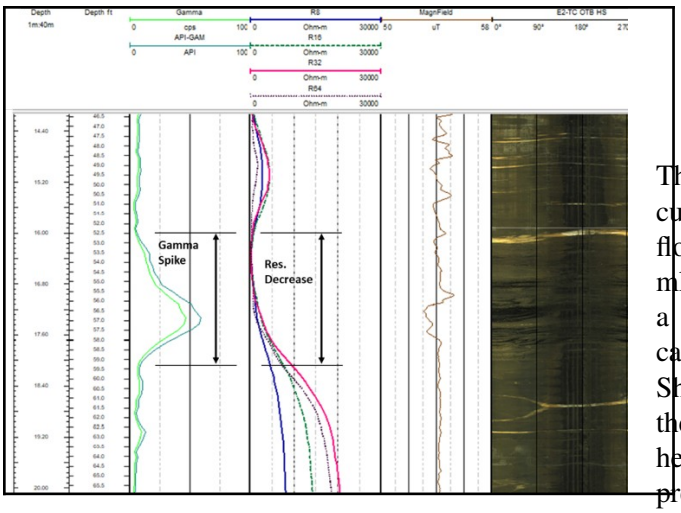

Figure 8: Resistivity – Gamma and Optical Borehole Imager log shows a gamma spike associated with a change in rock type and a resulting decrease in resistivity (Borehole E2-TC – planned injection well).

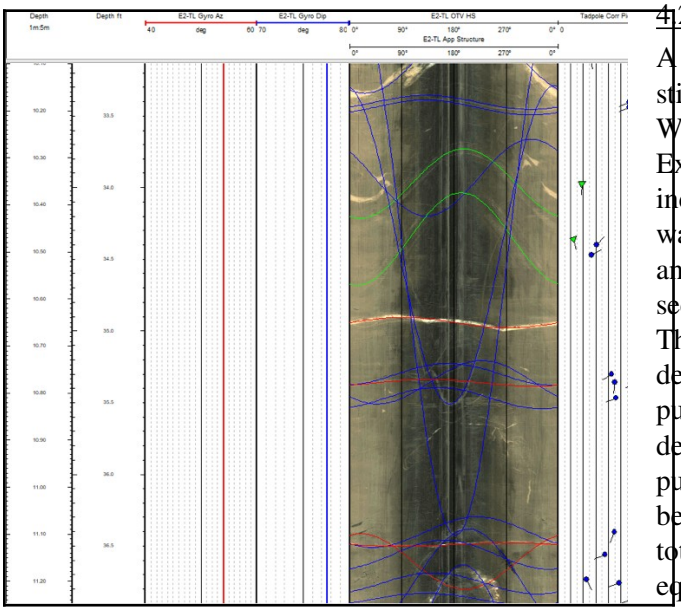

Figure 9: Optical borehole image log showing different types of features (green – foliation, blue – healed fractures/veins, and red – open fractures) (Borehole E2-TL, located beneath the planned injection well).

Other than the one flowing zone, careful monitoring of the inflows and outflows of the Experiment 2 boreholes during drilling showed:

- No evidence of connected fractures based on circulation during drilling (such fractures had been observed in Test Bed 1 at the 4850 level) and
- All flows were water losses *to* the rock except for E2-DMU and some initial outflows from E2-AML before it began losing water.

The water loss data following drilling show the cumulative losses over the drilling period give flow rates that range from approximately 20-180 ml/day. The water losses indicate flow to a sink at a lower elevation than the experiment. A likely candidate for the that sink is the nearby Yates Shaft. While the presence of flowing fractures in the vicinity of the test bed indicates highly heterogeneous fracture connectivity and pore pressure distributions, we expect the mine drainage is the main influence on pore pressures, and the pore pressure value is a relatively small, if not negligible fraction of the pressures required to open or stimulate fractures in the test bed.

4.2.2 Packer Hydraulic Characterization Tests

A major target of Experiment 2 is shear stimulation of a naturally conducting fracture. With only a few exceptions the fractures in the Experiment 2 test bed are healed and show little indication of being significantly transmissive. The water losses show the rock has some conductivity, and packer tests were performed to try to locate sections of preferential fracture transmissivity. The tests used a single low-pressure packer to determine hydraulic conductivity using pressure pulse tests, which allow evaluation of pressure decay after charging a test zone with a pressure pulse. The volume of flow into the test section can be determined from the pressure decay and the total compressibility of the test zone and the test equipment.

For these tests we used the regulated mine water pressure as pressure-pulse source (~0.5 MPa). Given the low conductivity of the rock, the pressure pulses decayed by only about 10% over the 30-minute test durations. The 30-minute pulse decay was followed by a 2-3 minute constant-rate injection. Data from the injection were used to obtain the total compressibility for calculating the

water loss to the borehole during the pulse decay period (Figure 10). Dividing this loss by the time-duration of the pulse gives a flow rate for calculation of transmissivity and hydraulic conductivity assuming steady state flow. The pressure pulse tests were performed over the entire open length of each borehole, except borehole E1-TC. In the E1-TC borehole the hydraulic characterization tests were conducted with the single packer located at depths of 30, 100, 150, and 200 ft (9.1, 30.5, 45.7, and 61.0 m.) to try to isolate transmissive candidate fractures for stimulation.

The pressure-pulse results (Table 2) show that the rock has a uniformly low permeability with total-borehole values ranging from 6.9×10^{-19} to 4.6×10^{-18} m^2 for most of the tests. The values for the borehole with the flowing zone, E2-DMU, are based on its measured flow of 180 ml/min and an assumed head of 1.4 MPa based on the measured pressure value in TV4100. The results of the four tests in E2-TC suggest that the bottom portion of the borehole (below 200 ft or 61 m) may be slightly more transmissive than the rest of the borehole.

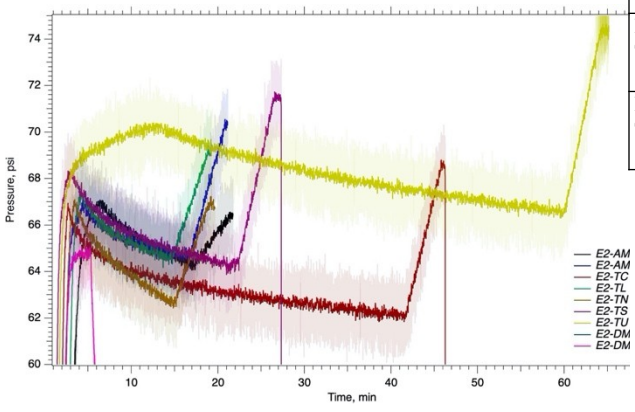

Figure 10. Pressure response of monitoring and test boreholes during hydraulic characterization test for Experiment 2.

Table 2. Hydraulic test results.

Borehole	Packer Set Depth (m)	Zone Length (m)	Transmissivity (m^2/s)	Hydraulic Conductivity (m/s)	Permeability (m^2)	Test Type
E2-TC	9.1	68.0	1.8E-09	2.7E-11	2.7E-18	Pressure-Pulse
E2-TU	9.1	67.4	4.7E-10	6.9E-12	6.9E-19	Pressure-Pulse
E2-TL	9.1	67.4	2.0E-09	2.9E-11	2.9E-18	Pressure-Pulse
E2-TN	9.1	67.4	3.1E-09	4.6E-11	4.6E-18	Pressure-Pulse
E2-TS	9.1	71.9	1.5E-09	2.1E-11	2.1E-18	Pressure-Pulse
E2-DML	9.1	46.0	1.5E-09	3.3E-11	3.3E-18	Pressure-Pulse
E2-DMU	9.1	45.7	2.2E-08	4.8E-10	4.8E-17	Steady Outflow
E2-AML	9.1	51.2	4.0E-09	7.9E-11	7.9E-18	Pressure-Pulse
E2-AMU	9.1	51.2	1.3E-09	2.5E-11	2.5E-18	Pressure-Pulse
E2-TC	30.5	46.6	1.5E-09	3.3E-11	3.3E-18	Pressure-Pulse
E2-TC	45.7	31.4	2.0E-09	6.5E-11	6.5E-18	Pressure-Pulse
E2-TC	61.0	16.2	2.2E-09	1.3E-10	1.3E-17	Pressure-Pulse

5. MONITORING SYSTEM

Although most of our monitoring system for Experiment 1 worked very well, the design of our monitoring system for Experiment 2 was informed by the observed pros and cons from our system for Experiment 1. We particularly sought to improve our microearthquake monitoring, robustness, and grouting of our boreholes. As with Experiment 1, the locations of our sensors were carefully evaluated prior to emplacement.

Design

The geophysical monitoring system consists of a comprehensive suite of downhole sensing instrumentation including active seismic, passive

seismic, fiber-based distributed temperature (DTS), strain (DSS), and acoustics (DAS), and electrical resistivity tomography (ERT), designed to provide autonomous and concurrent multi-parameter sensing during flow and stimulation operations. The sensor layout is shown in Figure 11. Downhole sensing components in the yellow boreholes aligned approximately orthogonal to the injection well are grouted in place. The remaining (blue and gray) monitoring boreholes are not grouted to enable geophysical monitoring instrumentation to be removed and replaced with flow testing instrumentation (e.g., packer systems and associated sensors) as needed to optimize testing objectives.

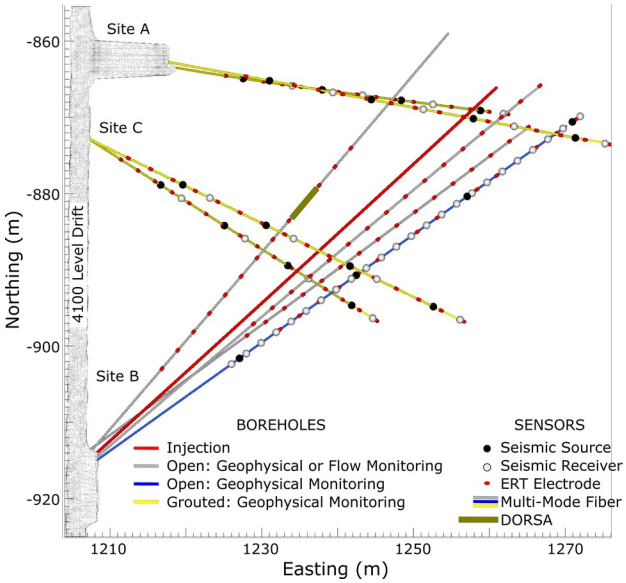

Figure 11. Plan view of geophysical monitoring borehole layout and sensor locations.

The instrumentation strings in each monitoring borehole were designed to reduce crosstalk between the seismic and ERT monitoring components, with a goal of enabling both to operate simultaneously. First, ERT electrodes and DTS/DAS/DSS fiber were attached outside a 2.5 in PVC shroud and advanced downhole as shown in Figure 12 (left). Second, a wellhead designed to seal the annulus during grouting was installed. Third, the seismic instrumentation string was installed on inside of the PVC shroud as shown in Figure 12 (right). The shroud was left open at the bottom of the borehole, which enables a grout return pathway through the inside of the PVC shroud to seal the seismic instrumentation in place. Finally, grout was pumped into the grout inlet (Figure 12) to fill the shroud and the annulus between the PVC shroud and borehole wall.

In comparison to the Experiment 1 design, many components were also hardened for increase durability during high pressure fracturing operations. Fiber optic components were deployed in very thin 316 stainless steel tubes (2.2 mm) coated in HDPE to prevent interference with ERT measurements. Seismic sensors (3C accelerometers) and sources (piezoelectric transducers) were also deployed on tubing encapsulated conductors (TEC: 4 mm, 316 stainless steel to prevent damage). Component seals were selected with ratings to at least 5000 psi.

Beyond rugged packaging, one key design improvement was inclusion of higher frequency 3-component (3C) accelerometer packages for microseismic monitoring. The selected 3C sensor (MMF, KS943B100[1]) is +- 3 dB to 22 kHz, providing a flat-frequency response to accurately capture the spectrum of small events. The unusual shape of this sensor (flat diamond) also necessitated the development of a custom sensor pod machined from 316 stainless steel, visible within the PVC shroud in Figure 12 (right). In total, 16 x 3C accelerometers are included in the microseismic array fully bracketing the planned stimulation zone. In addition to the accelerometer array, a dense array of 24 hydrophones was deployed in one of the production/monitoring wells to improve tomographic imaging coverage in the active source portion of the experiment

As mentioned before, the microseismic monitoring component of the experiment uses the 3C accelerometers in the four grouted monitoring wells, visible as green lines in Figure 13 surrounding the stimulation region with four accelerometers in each well, centered over the stimulation region.

Optimal accelerometer separation was determined before deployment by numerical modeling of microseismic hypocenter inversion. We obtain the

[1] Please see future updates for sensor performance.

relationships between the standard deviation error and the accelerometer interval for monitoring microseismic events around the stimulation region and those distributed in a region orthogonal to the stimulation well, as shown in Figure 13. We added Gaussian noise to synthetic travel time picks for event location analyses, to account for errors in the velocity models and travel time picks. Our numerical modeling suggested that the optimal receiver interval for the four geophones in each well is around 30-40 ft (~9.1-12.2 m), an estimate which guided the installation. The spacing of the ERT electrodes was also optimized in the design phase.

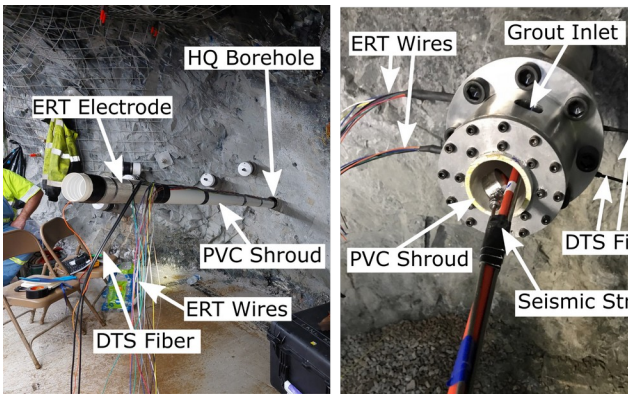

Figure 12. (left) Installation of ERT electrodes and DTS fiber on outside of monitoring well shroud. (Right) Installation of seismic instrument string on inside of monitoring well shroud.

The downhole robotic strain analyzer (DORSA) and Step-rate Injection Method for Fracture In-situ Properties (SIMFIP) (Guglielmi et al., 2015) tools will be used in Experiment 2. These borehole-based tools that measure strain in 3 dimensions across a fracture or fault. Both consist of a sensing element having six tendons in which strain is measured. Either side of the sensing element is stabilized against the nearby rock. Although there are many differences, for their use here the SIMFIP is placed between high pressure packers allowing measurement while stimulating under high-pressure. In its current embodiment, the DORSA is not a high-pressure tool, but suitable for use in low-pressure monitoring wells.

Grout design for monitoring wells

To preempt difficulties experienced in Experiment 1 with grouted boreholes, a new grout mixture was designed and tested. The grout used to secure the suite of instruments in the monitoring holes and to seal them preventing the movement of fluids along the length of the wells was designed to have electrical resistivity of approximately 1000 Ohm-m, the heat of hydration producing temperatures not exceeding the temperatures allowed by the installed instruments and their cables insulation (<80°C), and rheological parameters to easily flow into tight spaces between the cables and the equipment while still being stable and able to provide a tight seal against the cable insulation and a PVC pipe (no shrinkage) (Sollohub et al., 2022).

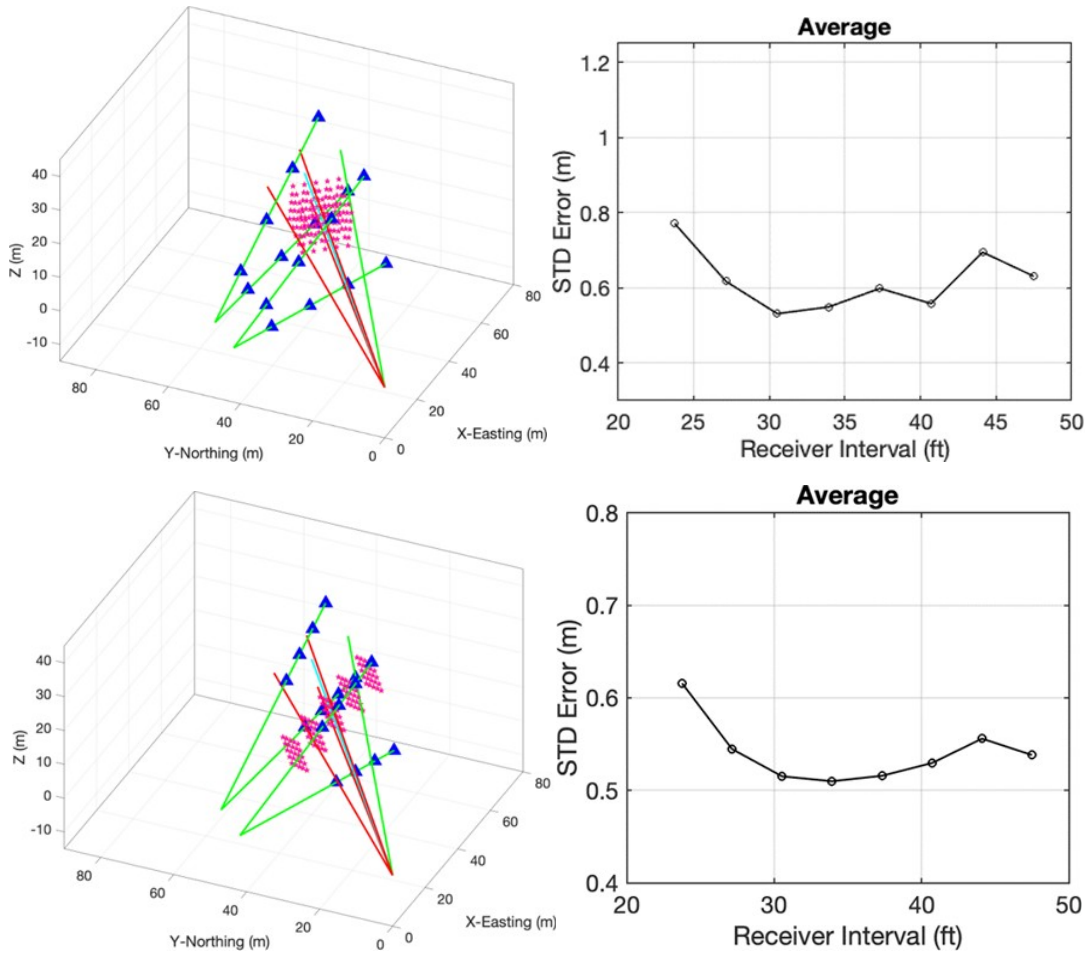

Figure 13: Top left panel: monitoring microseismic events (red stars) around the fracture stimulation region. Top right panel: The standard deviation error of microseismic event locations for the events in the top left panel vs. the receiver interval when using four accelerometers in each well, showing that the optimal receiver interval is around 30-40 ft. Bottom left panel: monitoring microseismic events (red stars) distributed in regions orthogonal to the stimulation well. Bottom right panel: The standard deviation error of microseismic event locations in the bottom left panel vs the receiver interval when using four accelerometers in each well, showing that the optimal receiver interval is also around 30-40 ft.

6. STIMULATION PLAN

Conceptual stimulation plans were formulated during the design and construction of the testbed. Once the testbed was complete, analyses were repeated based on all accumulated information, and stimulation plans were revised to address the goal of shear stimulation. This continued analysis led to the design of a mechanical system to effect the test stimulations and flows. This system was designed and built during the COVID pandemic and maximized remote system operation.

State of Stress

A principal objective of Experiment 2 is to shear stimulate a natural fracture within the testbed, creating a hydraulic connection between two test boreholes. Shear stimulation requires a natural fracture or plane of geologic discontinuity with moderate permeability oriented such that it is under a shearing stress. Shearing of the fracture surfaces occurs when fluid pressure within the fracture reduces the normal stress on the discontinuity sufficiently for the shear forces to overcome cohesive forces. The stress state within the testbed is currently uncertain, but two hypotheses have been developed to explain the non-vertical orientations of induced fractures

generated from stress measurements made in the vertical monitoring borehole TV4100 (Burghardt et al., 2020). The first hypothesis is that the minimum principal stress is dipped from horizontal, and the second is that there is a persistent plane of weakness, such as a natural fracture set, that yields induced fractures in that orientation. A Bayesian Markov Chain Monte Carlo uncertainty quantification analysis was completed to compute probability distributions for the principal stress magnitudes and orientations, based on elasticity solutions for the stress surrounding a vertical borehole with arbitrary principal stress magnitudes and directions. This analysis shows higher probabilities for tilted principal stress orientations (i.e., the principal vertical stress is not aligned with the gravitational direction). The stress orientation and magnitudes provide information about the shear stresses on natural fractures identified in the test boreholes. Fracture permeability data (Table 2) are also needed to identify a natural fracture as having slip potential. Detailed core and borehole televiewer observations were also made to identify prospective fractures that may connect the injection borehole (E2-TC) with one or more of the surrounding production boreholes. Few obvious candidates were observed. Another complicating feature is that almost all of the fractures are mineralized, which might make shear stimulation of such features more challenging (e.g., Meng et al. (2021a)).

Stimulation Design

Because few fractures with significant permeability were identified, the planned stimulation protocol focuses on fractures with the highest shear-to-normal stress. Figure 14 shows lower hemisphere pole plots of the fractures in E1-TC identified with each fracture being colored according to the expected value of the shear to mean stress ratio for these two stress state hypotheses. As the figure shows, the shear-to-normal stress ratio is relatively low, with the highest values being approximately 0.25 and 0.35 for the two stress hypotheses. This contrasts with a nominally expected critical friction coefficient of 0.6, which means that even in the absence of significant cohesion no fractures are expected to be close to incipient shear failure.

The planned stimulations will target a few fractures with the highest shear-to-normal stress for each stress state hypothesis. Each targeted fracture will be isolated with a straddle packer assembly and then subjected to 500 psi (3.5 MPa) until the flow rate reaches steady state. This step is to characterize the initial hydraulic properties of the fracture in a more detailed manner than the prior lower pressure hydraulic characterization tests. Next, the zone will be pressurized to 2200 psi (15.2 MPa), which is approximately 83% of the minimum expected value of the minimum principal stress and only 30% of the well pressure that is estimated to be required to generate a tensile stress at the borehole wall. This pressure is therefore very unlikely to initiate a tensile hydraulic fracture. Any increase in permeability of the zone will therefore be a strong indication of shear stimulation. Measurements using the SIMFIP tool (Guglielmi et al., 2014) will also quantify shear displacement. Because of the expected low permeability of the targeted natural fractures, a significant amount of time may be required to allow the applied pressure to diffuse into the natural fracture and initiate shear slip. It is planned to hold several of the fractures under pressure for two weeks to provide the best possible chance of shear stimulation.

Stimulation System Design

The stimulation and flow system for Experiment 2 was designed to be robust, reliable, remote-controlled, and modular (Ingraham et al., 2021). With those guiding principles and a few design constraints including the small alcove footprint, flow rates of ~13 Lpm, and pressures of up to ~ 50 MPa, a few fundamental design decisions were made. To minimize head losses while maintaining relatively small plumbing components, an orifice diameter of ~12 mm was selected. These constraints led to selection of plumbing standards, as well as the plumbing design, which was kept being as two dimensional as possible to minimize its footprint in the narrow drift. Modularity of the system was needed because there are 5 boreholes that could be used for injection or production. This means that each of the borehole

injection/production lines has identical plumbing, lines, and packer systems. This provides for robust design in that there are a minimal number of spare parts required for the system, and should one panel fail, one of the others could be used to replace it until parts are available. An example of the modular plumbing is shown in Figure 15. Figure 16 shows the system installed on the 4100 level.

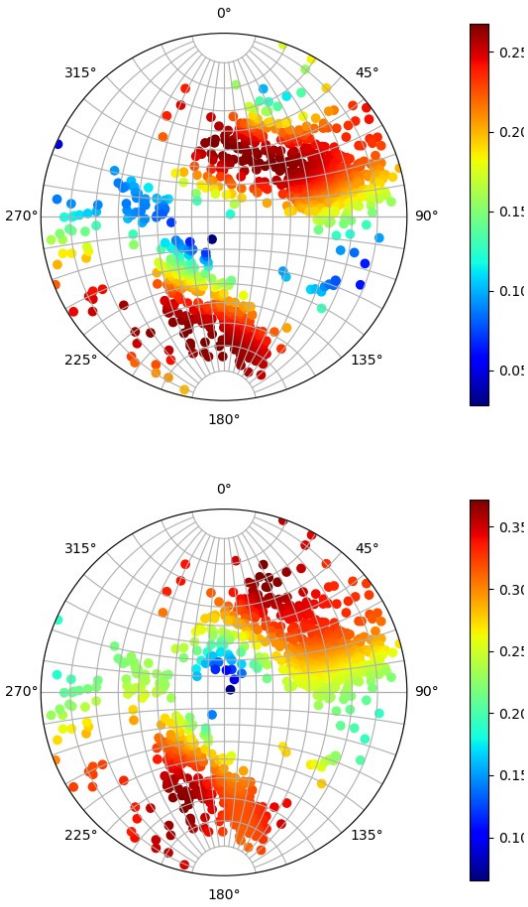

Figure 14. Top - Equal angle lower hemisphere projection of poles of identified fractures in E2-TC, colored according to the mean shear-to-normal stress ratio under the hypothesis that the principal stresses are rotated from vertical/horizontal. Bottom - Equal angle lower hemisphere projection of poles of identified fractures in E2-TC, colored according to the mean shear-to-normal stress ratio under the assumption that the principal stresses are vertical/horizontal.

The system can be operated remotely from anywhere with internet access. Although many will be able to view the data in real time on another system, control of the system is limited to specific individuals who can remotely access the control computer from outside the mine and change pressures/flows/valving. This allows for the required number of people to have access and monitor the system 24/7 and change flow parameters as needed. This includes the ability to run the supply fluid through a reverse osmosis system to reduce the conductivity of the injected water to inject this “tracer” at any time or change the temperature of the injected water. The control system is built with a custom LabVIEW VI, and control is implemented with National Instruments hardware.

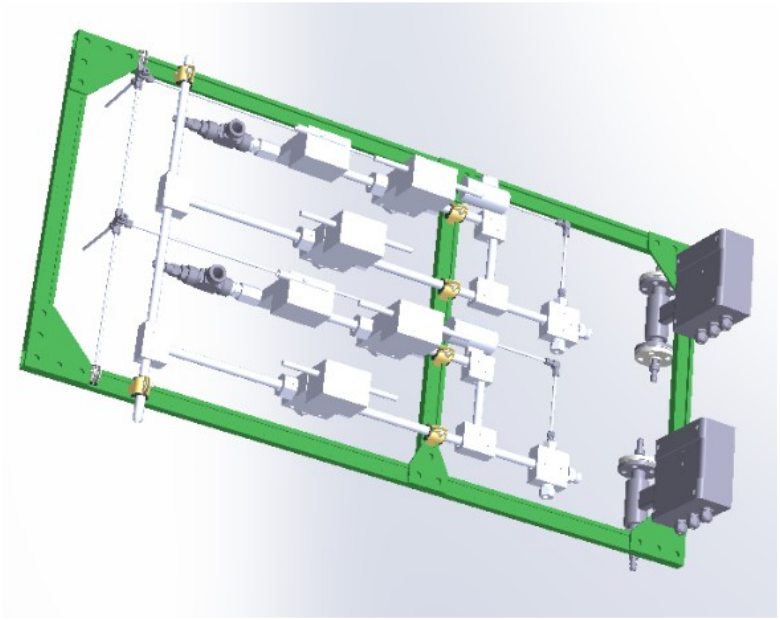

Figure 15: CAD model of the modular plumbing for one of the packer systems.

Figure 16: Panoramic of the system as installed on the 4100 level. Note the modular plumbing hung on the wall behind the other equipment and the control computer.

7. CONCLUDING REMARKS

The EGS Collab project Experiment 1 has been completed, and data and papers are readily available. The Experiment 2 testbed is in a stress, rock type, and natural fractured environment that is significantly different from Experiment 1. The Experiment 2 design considers the complex geology including stress and fracture set orientations, types of fractures and whether they are healed, and the presence of a lower-stress rhyolite layer. Spatial constraints from working in a smaller drift and the drift orientation were addressed by design. Lessons learned from Experiment 1 including increasing spacing between the monitoring wells, ruggedizing sensors, and customizing the grout for monitoring wells were also incorporated into Experiment 2 design. The new testbed contains an injection well surrounded by four production wells, all of which will be used for monitoring flows and pressures. These wells are optimally placed within the densely instrumented test bed and are oriented to intersect fractures most likely to shear. Our geophysical monitoring tools are optimized for the testbed and the experiment and are expected to provide excellent high-resolution data to allow observing and quantifying processes that occur during the experiment. Tools explicitly designed to measure shear including the SIMFIP and DORSA tools and DAS will be used both in the stimulation well and also in the surrounding wells, and ERT is expected to show changes in the system. The optimized mechanical system built for this experiment addresses concerns learned in Experiment 1 and can almost entirely be operated remotely once packers are placed. We will again have the ability to broadcast data immediately and remotely change experiment parameters.

We expect to face many challenges. The healed nature of most fractures is expected to hinder shear stimulation, as is the shear-to-normal stress ratio. Our stimulation strategy, however, has multiple contingencies for execution that will be pragmatically employed based depending on observations during testing. Our improved testbed design and novel instrumentation capabilities provide substantial experiment flexibility and rapid decision-making power to overcome these challenges while conducting this series of 10-m scale EGS tests.

8. ACKNOWLEDGMENTS

This material was based upon work supported by the U.S. Department of Energy, Office of Energy Efficiency and Renewable Energy (EERE), Office of Technology Development, Geothermal Technologies Office, under Award Number DE-AC02-05CH11231 with LBNL and other awards to other national laboratories. The United States Government retains, and the publisher, by accepting the article for publication, acknowledges that the United States Government retains a non-exclusive, paid-up, irrevocable, world-wide license to publish or reproduce the published form of this manuscript, or allow others to do so, for United States Government purposes.

Sandia National Laboratories is a multimission laboratory managed and operated by National Technology & Engineering Solutions of Sandia, LLC, a wholly owned subsidiary of Honeywell International Inc., for the U.S. Department of Energy's National Nuclear Security Administration under contract DE-NA0003525. This paper describes objective technical results and analysis. Any subjective views or opinions that might be expressed in the paper do not necessarily represent the views of the U.S. Department of Energy or the United States Government. The research supporting this work took place in whole or in part at the Sanford Underground Research Facility in Lead, South Dakota. The assistance of the Sanford Underground Research Facility and its personnel in providing physical access and general logistical and technical support is gratefully acknowledged. We also thank the crew from RESPEC, who logged the core upon recovery from drilling, and also supported the wireline logging operations. The earth model output for this paper was generated using Leapfrog Software, copyright Seequent Limited. Leapfrog and all other Seequent Limited product or service names are registered trademarks or trademarks of Seequent Limited.

9. REFERENCES

1. Ajo-Franklin, J. B., Schoenball, M., Wood, T., Robertson, M., Petrov, P., Huang, L., Kneafsey, T. J., Schwering, P., Blankenship, D., Knox, H., & EGS Collab Team. (2018). *Imaging Hydraulic Fracture Propagation Using Semi-Permanent Continuous Active Seismic Source Monitoring: Results from the DOE EGS Collab Experiment*. Paper presented at the American Geophysical Union Fall Meeting 2018, Washington DC.
2. Augustine, C. (2016). Update to Enhanced Geothermal System Resource Potential Estimate. *GRC Transactions, 40*, 6.
3. Burghardt, J., Doe, T., Ingraham, M., Schwering, P., Ulrich, C., Roggenthen, W. M., Reimers, C., & EGS Collab Team. (2020). *Integration of Shut-In Pressure Decline, Flow back, Hydraulic and Sleeve Re-Opening Tests to Infer In-Situ Stress.* Paper presented at the 54th U.S. Rock Mechanics/Geomechanics Symposium.
4. Burghardt, J., Knox, H. A., Doe, T., Blankenship, D., Schwering, P. C., M., I., Kneafsey, T. J., Dobson, P. F., Ulrich, C., Guglielmi, Y., & Roggenthen, W. (2022). *EGS Stimulation Design with Uncertainty Quantification at the EGS Collab Site*. Paper presented at the 56th US Rock Mechanics/Geomechanics Symposium, Santa Fe, New Mexico, USA.
5. Caddey, S. W., Bachman, R. L., Campbell, T. J., Reid, R. R., & Otto, R. P. (1991). *The Homestake gold mine, an early Proterozoic iron-formation-hosted gold deposit, Lawrence County, South Dakota* (1857J). Retrieved from http://pubs.er.usgs.gov/publication/b1857J
6. Chai, C., Maceira, M., Santos-Villalobos, H. J., Venkatakrishnan, S. V., Schoenball, M., & EGS Collab Team. (2020). *Automatic Seismic Phase Picking Using Deep Learning for the EGS Collab project*. Paper presented at the 45th Workshop on Geothermal Reservoir Engineering, Stanford University, Stanford, California.
7. Chi, B., Huang, L., Gao, K., Ajo-Franklin, J., Kneafsey, T. J., Hampton, J., & EGS Collab Team. (2020). *Anisotropic Imaging of Created Fractures in EGS Collab Experiments Using CASSM Data*. Paper presented at the 45th Workshop on Geothermal Reservoir Engineering, Stanford University, Stanford, California.
8. Dobson, P., Kneafsey, T., Morris, J., Singh, A., Zoback, M., Roggenthen, W., Doe, T., Neupane, G., Podgorney, R., Wang, H., Knox, H., Schwering, P., Blankenship, D., Ulrich, C., Johnson, T., White, M., & EGS Collab Team. (2018). *The EGS Collab Hydroshear Experiment at the Sanford Underground Research Facility – Siting Criteria and Evaluation of Candidate Sites*. Paper presented at the Geothermal Resources Council 2018 Annual Meeting, Reno, NV.
9. Dobson, P., Kneafsey, T. J., Blankenship, D., Morris, J., Fu, P., Knox, H., Schwering, P., Ingraham, M., White, M., Johnson, T., Burghardt, J., Doe, T., Roggenthen, W., Neupane, G., Podgorney, R., Horne, R., Hawkins, A., Singh, A., Huang, L., Frash, L., Weers, J., Ajo-Franklin, J., Schoenball, M., Ulrich, C., Mattson, E., Uzunlar, N., Valladao, C., & EGS Collab Team. (2021). *The EGS Collab Project – Fracture Stimulation and Flow Experiments for Coupled Process Model Validation at the Sanford Underground Research Facility (SURF), South Dakota, USA*. Paper presented at the World Geothermal Congress 2020+1 Reykjavik, Iceland.
10. Fu, P., Schoenball, M., Morris, J., Ajo-Franklin, J., Knox, H., Kneafsey, T., Burghardt, J., White, M., & EGS Collab Team. (2019). *Microseismic Signatures of Hydraulic Fracturing: A Preliminary Interpretation of Intermediate-Scale Data from the EGS Collab Experiment*. Paper presented at the 44th Workshop on Geothermal Reservoir Engineering, Stanford University, Stanford, California.
11. Fu, P., Wu, H., Morris, J. P., Schwering, P. C., Ulrich, C., Burghardt, J. A., Ingraham, M. D., Doe, T. W., & EGS Collab Team. (2021). *Simulating Hydraulic Fracture Stimulations at the EGS Collab: Model Validation from Experiments 1 and Design-Phase Simulation for Experiment 2*. Paper presented at the 46th Workshop on Geothermal Reservoir Engineering, Stanford University, Stranford, CA.
12. Guglielmi, Y., Cappa, F., Avouac, J.-P., Henry, P., & Elsworth, D. (2015). Seismicity triggered by fluid

injection–induced aseismic slip. *Science, 348*(6240), 1224.

13. Guglielmi, Y., Cook, P., Soom, F., Dobson, P., Kneafsey, T., Valley, B., Kakurina, M., Niemi, A., Tsang, C. F., Tatomir, A., Juhlin, C., & Basirat, F. (2021a). *Estimating Stress from Three-Dimensional Borehole Displacements Induced by Fluid Injection in Different Types of Fractured or Faulted Rocks*. Paper presented at the 55th US Rock Mechanics/Geomechanics Symposium, Houston, Texas, USA.
14. Guglielmi, Y., Cook, P., Soom, F., Schoenball, M., Dobson, P., & Kneafsey, T. (2021b). In Situ Continuous Monitoring of Borehole Displacements Induced by Stimulated Hydrofracture Growth. *Geophysical Research Letters, 48*, e2020GL090782. doi:https://doi.org/10.1029/2020GL090782
15. Guglielmi, Y., McClure, M., Burghardt, J., Morris, J. P., Doe, T., Fu, P., Knox, H., Vermeul, V., Kneafsey, T., & EGS Collab Team. (2022). *Estimating Stress from Fracture Injection Tests: Comparing Pressure Transient Interpretations with In-Situ Strain Measurements*. Paper presented at the 47th Workshop on Geothermal Reservoir Engineering, Stanford University, Stanford, California.
16. Guglielmi, Y. G., Cappa, F., Rutqvist, J., Tsang, C. F., Wang, J., Lançon, H., Durand, J., & Janowczyk, J. B. (2014). *Step-Rate Injection Method for Fracture In-Situ Properties (SIMFIP): Monitoring Fractures Stimulation Efficiency*. Paper presented at the 48th U.S. Rock Mechanics/Geomechanics Symposium, Minneapolis, Minnesota.
17. Heise, J. (2015). The Sanford Underground Research Facility at Homestake. *Journal of Physics: Conference Series, 606*(1), 26.
18. Ingraham, M., Strickland, C., Vermuel, V., Roberts, B., Burghardt, J., Schwering, P., Knox, H., & ., E. C. T. (2021). Design and fabrication of a remote-control hydraulic fracturing system. *GRC Transactions, 45, 686-693.*, 8.
19. Ingraham, M. D., Schwering, P. C., Burghardt, J., Ulrich, C., Doe, T., Roggenthen, W. M., & Reimers, C. (2020). *Analysis of Hydraulic Fracturing on the 4100 Level at the Sanford Underground Research Facility*. Paper presented at the 54th U.S. Rock Mechanics/Geomechanics Symposium. https://doi.org/
20. Jafarov, E. E., Makedonska, N., Karra, S., Pawar, R., Beisman, J., Neupane, G., Schwering, P. C., Kneafsey, T. J., & EGS Collab Team. (2020). *Simulations of the 3D Geothermal Heat Flow in Fractured Media*. Paper presented at the 45th Workshop on Geothermal Reservoir Engineering, Stanford University, Stanford, California.
21. Johnson, T., Strickland, C., Knox, H., Thomle, J., Vermuel, V., Ulrich, C., Kneafsey, T., Blankenship, D., & EGS Collab Team. (2019). *EGS Collab Project Electrical Resistivity Tomography Characterization and Monitoring Status*. Paper presented at the 44th Workshop on Geothermal Reservoir Engineering, Stanford University, Stanford, California.
22. Johnson, T. C., Burghardt, J., Strickland, C., Knox, H., Vermeul, V., White, M., Schwering, P., Blankenship, D., & EGS Collab Team. (2021). 4D Proxy Imaging of Fracture Dilation and Stress Shadowing Using Electrical Resistivity Tomography During High Pressure Injections Into a Dense Rock Formation. *Journal of Geophysical Research: Solid Earth, 126*(11), e2021JB022298. doi:https://doi.org/10.1029/2021JB022298
23. Kneafsey, T., Blankenship, D., Dobson, P., White, M., Morris, J. P., Fu, P., Wu, H., Schwering, P. C., Ajo-Franklin, J. B., Huang, L., Knox, H. A., Neupane, G., Weers, J., Horne, R., Roggenthen, W., Doe, T., & EGS Collab Team. (2021). *Fracture Stimulation and Chilled-water Circulation Through Deep Crystalline Rock: Characterization, Modeling, Monitoring, and Heat-transfer Assessment*. Paper presented at the 46th Workshop on Geothermal Reservoir Engineering, Stanford University, Stanford, California.
24. Kneafsey, T. J., Blankenship, D., Dobson, P. F., Morris, J. P., White, M. D., Fu, P., Schwering, P. C., Ajo-Franklin, J. B., Huang, L., Schoenball, M., Johnson, T. C., Knox, H. A., Neupane, G., Weers, J., Horne, R., Zhang, Y., Roggenthen, W., Doe, T., Mattson, E., Valladao, C., & EGS Collab Team. (2020). *The EGS Collab Project: Learnings from Experiment 1*. Paper presented at the 45th Workshop on Geothermal Reservoir Engineering, Stanford University, Stanford, California.
25. Lisenbee, A. L., & Terry, M. (2009). *Development of a 3-D structural geology model of Homestake's 4100 to 5000 levels at the proposed location of the large cavities* (SDSMT Contract #09-05). Retrieved from
26. Makedonska, N., Jafarov, E., Doe, T., Schwering, P., Neupane, G., & EGS Collab Team. (2020). *Simulation of Injected Flow Pathways in Geothermal Fractured Reservoir Using Discrete Fracture Network Model*. Paper presented at the 45th Workshop on Geothermal Reservoir Engineering, Stanford University, Stanford, California.
27. Mattson, E., Neupane, G., Hawkins, A., Burghardt, J., Ingraham, M., Plummer, M., & EGS Collab Team. (2019a). Fracture Tracer Injection Response to Pressure Perturbations at an Injection Well. *GRC Transactions, 43*.
28. Mattson, E., Zhang, Y., Hawkins, A., Johnson, T., Ajo-Franklin, J., Neupane, G., & EGS Collab Team. (2019b). *Preliminary Collab Fracture Characterization Results from Flow and Tracer Testing Efforts* Paper presented at the 44th Workshop on Geothermal Reservoir Engineering, Stanford University, Stanford, California.
29. Meng, M., Frash, L. P., Li, W., Welch, N. J., & Carey, J. W. (2021a). *Measurement of Geomechanical and Hydrological Properties of EGS-Collab Geothermal Rocks*. Paper presented at the 55th US Rock Mechanics/ Geomechanics Symposium, Houston, Texas, USA.
30. Meng, M., Frash, L. P., Li, W., Welch, N. J., Carey, J. W., Ulrich, C., & Kneafsey, T. J. (2021b). Hydro-mechanical measurements of sheared crystalline rock fractures with applications for EGS Collab experiments

1 & 2. *Journal of Geophysical Research - Solid Earth, accepted*.

31. Morris, J. P. (2021). Fat Crayon Toolkit. https://www.osti.gov/biblio/1764513.
32. Morris, J. P., Fu, P., Dobson, P., Ajo-Franklin, J., Kneafsey, T. J., Knox, H., Blankenship, D., White, M. D., Burghardt, J., Doe, T. W., & EGS Collab Team. (2018). *Experimental Design for Hydrofracturing and Fluid Flow at the DOE EGS Collab Testbed*. Paper presented at the 52nd US Rock Mechanics / Geomechanics Symposium, Seattle, Washington, USA.
33. Neupane, G., Mattson, E. D., Plummer, M. A., & EGS Collab Team. (2020). *Results of Multiple Tracer Injections into Fractures in the EGS Collab Testbed-1*. Paper presented at the 45th Workshop on Geothermal Reservoir Engineering, Stanford University, Stanford, California.
34. Oldenburg, C. M., Dobson, P. F., Wu, Y., Cook, P. J., Kneafsey, T. J., Nakagawa, S., Ulrich, C., Siler, D. L., Guglielmi, Y., Ajo-Franklin, J., Rutqvist, J., Daley, T. M., Birkholzer, J. T., Wang, H. F., Lord, N. E., Haimson, B. C., Sone, H., Vigilante, P., Roggenthen, W. M., Doe, T. W., Lee, M. Y., Ingraham, M., Huang, H., Mattson, E. D., Zhou, J., Johnson, T. J., Zoback, M. D., Morris, J. P., White, J. A., Johnson, P. A., Coblentz, D. D., & Heise, J. (2017). *Hydraulic fracturing experiments at 1500 m depth in a deep mine: Highlights from the kISMET project*. Paper presented at the 42nd Workshop on Geothermal Reservoir Engineering, Stanford University.
35. Pan, W., Huang, L., Gao, K., Ajo-Franklin, J., Kneafsey, T. J., & EGS Collab Team. (2019). *Anisotropic Full-Waveform Inversion and Least-Squares Reverse-Time Migration of CASSM Data for Experiment I of the EGS Collab Project* Paper presented at the 44th Workshop on Geothermal Reservoir Engineering, Stanford University, Stanford, California.
36. Schoenball, M., Ajo-Franklin, J., Blankenship, D., Cook, P., Dobson, P., Guglielmi, Y., Fu, P., Kneafsey, T., Knox, H., Petrov, P., Robertson, M., Schwering, P., Templeton, D., Ulrich, C., Wood, T., & EGS Collab Team. (2019). *Microseismic monitoring of meso-scale stimulations for the DOE EGS Collab project at the Sanford Underground Research Facility*. Paper presented at the 44th Workshop on Geothermal Reservoir Engineering, Stanford University, Stanford, California.
37. Schoenball, M., Ajo-Franklin, J. B., Blankenship, D., Chai, C., Chakravarty, A., Dobson, P., Hopp, C., Kneafsey, T., Knox, H. A., Maceira, M., Robertson, M. C., Sprinkle, P., Strickland, C., Templeton, D., Schwering, P. C., Ulrich, C., Wood, T., & EGS Collab Team. (2020a). Creation of a Mixed-Mode Fracture Network at Mesoscale Through Hydraulic Fracturing and Shear Stimulation. *Journal of Geophysical Research: Solid Earth, 125*(12), e2020JB019807. doi:https://doi.org/10.1029/2020JB019807
38. Schoenball, M., Ajo-Franklin, J. B., Wood, T., Robertson, M., Cook, P., Rodriguez-Tribaldos, V., Crowe, D., Hao, Z., Kneafsey, T., & EGS Collab Team. (2020b). *Lessons learned from passive seismic monitoring of EGS Collab Experiment 1*. Paper presented at the 45th Workshop on Geothermal Reservoir Engineering, Stanford University, Stanford, California.
39. Schoenball, M., Guglielmi, Y., Ajo-Franklin, J. B., Cook, P. J., Dobson, P., Hopp, C., Kneafsey, T. J., Soom, F., & Ulrich, C. (2021). In-situ observation of pre-, co-and post-seismic shear slip at 1.5 km depth. *Earth and Space Science Open Archive* doi:10.1002/essoar.10506700.1
40. Singh, A., Zoback, M., Dobson, P. F., Kneafsey, T. J., Schoenball, M., Guglielmi, Y., Ulrich, C., Roggenthen, W., Uzunlar, N., Morris, J., Fu, P., Schwering, P. C., Knox, H. A., Frash, L., Doe, T. W., Wang, H., Condon, K., Johnston, B., & EGS Collab Team. (2019). Slip tendency analysis of fracture networks to determine suitability of candidate testbeds for the EGS Collab hydroshear experiment. *Geothermal Resources Council Transactions, 43*, 405–424.
41. Sollohub, L., Johnson, T., Sugama, T., & Pyatina, T. (2022). *High Resistivity Well Cement for Underground Wells Suitable for Sealing Monitoring Equipment*. Paper presented at the 47th Workshop on Geothermal Reservoir Engineering, Stanford University, Stanford, California.
42. Stetler, L. D. (2015). *Water geochemistry and pressure buildup in drill holes on the 4950-ft level at the Sanford Underground Research Facility*. Paper presented at the Proceedings of the South Dakota Academy of Sciences.
43. Templeton, D., Morris, J., Schoenball, M., Wood, T., Robertson, M., Cook, P., Dobson, P., Ulrich, C., Ajo-Franklin, J., Kneafsey, T., Schwering, P., Blankenship, D., Knox, H., & EGS Collab Team. (2019). *Microseismic Correlation and Cluster Analysis of DOE EGS Collab Data*. Paper presented at the 44th Workshop on Geothermal Reservoir Engineering, Stanford University, Stanford, California.
44. Ulrich, C., Dobson, P. F., Kneafsey, T. J., Roggenthen, W. M., Uzunlar, N., Doe, T. W., Neupane, G., Podgorney, R., Schwering, P., Frash, L., Singh, A., & EGS Collab Team. (2018). *The Distribution, Orientation, and Characteristics of Natural Fractures for Experiment 1 of the EGS Collab Project, Sanford Underground Research Facility*. Paper presented at the 52nd U.S. Rock Mechanics/Geomechanics Symposium, Seattle, Washington.
45. Wang, H. F., Lee, M. Y., Doe, T. W., Haimson, B. C., Oldenburg, C. M., & Dobson, P. F. (2017). *In-Situ Stress Measurement at 1550-Meters Depth at the kISMET Test Site in Lead, S.D*. Paper presented at the 51st U.S. Rock Mechanics/Geomechanics Symposium, San Francisco, California, USA.
46. White, M., Johnson, T., Kneafsey, T., Blankenship, D., Fu, P., Wu, H., Ghassemi, A., Lu, J., Huang, H., Neupane, G., Oldenburg, C., Doughty, C., Johnston, B., Winterfeld, P., Pollyea, R., Jayne, R., Hawkins, A., Zhang, Y., & EGS Collab Team. (2019). *The Necessity for Iteration in the Application of Numerical Simulation to EGS: Examples from the EGS Collab Test Bed 1*. Paper presented at the 44th Workshop on Geothermal

Reservoir Engineering, Stanford University, Stanford, California.
47. White, M. D., Burghardt, J. A., & EGS Collab Team. (2021). *Modeling the Dynamic Flow Resistance Across the Fracture Network of EGS Collab Experiment 1*. Paper presented at the 46th Workshop on Geothermal Reservoir Engineering, Stanford University, Stanford, California.
48. White, M. D., Fu, P., & EGS Collab Team. (2020). *Application of an Embedded Fracture and Borehole Modeling Approach to the Understanding of EGS Collab Experiment 1*. Paper presented at the 45th Workshop on Geothermal Reservoir Engineering, Stanford University, Stanford, California.
49. White, M. D., Fu, P., Ghassemi, A., Huang, H., Rutqvist, J., Johnston, B., & EGS Collab Team. (2018). *Numerical Simulation Applications in the Design of EGS Collab Experiment 1*. Paper presented at the 43rd Workshop on Geothermal Reservoir Engineering, Stanford University, Stanford, California.
50. Williams, C. F., Reed, M. J., Mariner, R. H., DeAngelo, J., & Galanis, S. P., Jr. (2008). *Assessment of moderate- and high-temperature geothermal resources of the United States*. (United States Geological Survey Fact Sheet 2008-3082).
51. Wu, H., Fu, P., Morris, J. P., Settgast, R. R., Ryerson, F. J., Mattson, E. D., Hawkins, A. J., & Zhang, Y. (2019). *Stochastic modeling of a conservative tracer test for the characterization of fracture flow patterns in EGS Collab Experiment 1*. Paper presented at the 53rd US Rock Mechanics/Geomechanics Symposium, New York, NY, USA.
52. Zhan, G., & Duex, T. (2010). Hydrologic evaluation of post-closure flooding and dewatering of the Homestake Mine. *Mining Engineering, April*, 5.

J. Ajo-Franklin, T. Baumgartner, K. Beckers, D. Blankenship, A. Bonneville, L. Boyd, S. Brown, J.A. Burghardt, C. Chai, A. Chakravarty, T. Chen, Y. Chen, B. Chi, K. Condon, P.J. Cook, D. Crandall, P.F. Dobson, T. Doe, C.A. Doughty, D. Elsworth, J. Feldman, Z. Feng, A. Foris, L.P. Frash, Z. Frone, P. Fu, K. Gao, A. Ghassemi, Y. Guglielmi, B. Haimson, A. Hawkins, J. Heise, C. Hopp, M. Horn, R.N. Horne, J. Horner, M. Hu, H. Huang, L. Huang, K.J. Im, M. Ingraham, E. Jafarov, R.S. Jayne, T.C. Johnson, S.E. Johnson, B. Johnston, S. Karra, K. Kim, D.K. King, T. Kneafsey, H. Knox, J. Knox, D. Kumar, K. Kutun, M. Lee, D. Li, J. Li, K. Li, Z. Li, M. Maceira, P. Mackey, N. Makedonska, C.J. Marone, E. Mattson, M.W. McClure, J. McLennan, T. McLing, C. Medler, R.J. Mellors, E. Metcalfe, J. Miskimins, J. Moore, C.E. Morency, J.P. Morris, T. Myers, S. Nakagawa, G. Neupane, G. Newman, A. Nieto, T. Paronish, R. Pawar, P. Petrov, B. Pietzyk, R. Podgorney, Y. Polsky, J. Pope, S. Porse, J.C. Primo, T. Pyatina, C. Reimers, B.Q. Roberts, M. Robertson, V. Rodríguez-Tribaldos, W. Roggenthen, J. Rutqvist, D. Rynders, M. Schoenball, P. Schwering, V. Sesetty, C.S. Sherman, A. Singh, M.M. Smith, H. Sone, E.L. Sonnenthal, F.A. Soom, D.P. Sprinkle, S. Sprinkle, C.E. Strickland, J. Su, D. Templeton, J.N. Thomle, C. Ulrich, N. Uzunlar, A. Vachaparampil, C.A. Valladao, W. Vandermeer, G. Vandine, D. Vardiman, V.R. Vermeul, J.L. Wagoner, H.F. Wang, J. Weers, N. Welch, J. White, M.D. White, P. Winterfeld, T. Wood, S. Workman, H. Wu, Y.S. Wu, E.C. Yildirim, Y. Zhang, Y.Q. Zhang, Q. Zhou, M.D. Zoback